Exploration of Cobalt@N-doped Carbon Nanocomposites toward Hydrogen Peroxide(H_2O_2) Electrosynthesis: a two level investigation through the RRDE analysis and a polymer-based electrolyzer implementation

Marcello Ferrara , Manuela Bevilacqua , Michele Melchionna , Alejandro Criado , Matteo Crosera , Claudio Tavagnacco , Francesco Vizza , Paolo Fornasiero

PII: S0013-4686(20)31680-7
DOI: https://doi.org/10.1016/j.electacta.2020.137287
Reference: EA 137287

To appear in: *Electrochimica Acta*

Received date: 18 August 2020
Revised date: 8 October 2020
Accepted date: 12 October 2020

Please cite this article as: Marcello Ferrara , Manuela Bevilacqua , Michele Melchionna , Alejandro Criado , Matteo Crosera , Claudio Tavagnacco , Francesco Vizza , Paolo Fornasiero , Exploration of Cobalt@N-doped Carbon Nanocomposites toward Hydrogen Peroxide(H_2O_2) Electrosynthesis: a two level investigation through the RRDE analysis and a polymer-based electrolyzer implementation, *Electrochimica Acta* (2020), doi: https://doi.org/10.1016/j.electacta.2020.137287

Highlights

1) Cobalt-carbon core shells were established to be highly selective for 2 e^- ORR pathway.
2) Co encapsulated N-carbon was used as electrocatalyst for the selective H_2O_2 formation.
3) Rotating Ring Disc Electrode was used to rationalize structure/activity relationship.
4) The electrode implementation in a PEM static flow electrolyzer setup was investigated.

Exploration of Cobalt@N-doped Carbon Nanocomposites toward Hydrogen Peroxide(H_2O_2) Electrosynthesis: a two level investigation through the RRDE analysis and a polymer-based electrolyzer implementation

Marcello Ferrara,[a] Manuela Bevilacqua,[b,c,*] Michele Melchionna,[a] Alejandro Criado,[d] Matteo Crosera,[a] Claudio Tavagnacco,[a] Francesco Vizza,[c] Paolo Fornasiero[a,b,*]

[a] Department of Chemical and Pharmaceutical Sciences, University of Trieste and Consortium INSTM, Via L. Giorgieri 1, 34127 Trieste, Italy.

[b] ICCOM-CNR, University of Trieste, Via L. Giorgieri 1, 34127 Trieste, Italy.

[c] ICCOM-CNR, via Madonna del Piano 10, 50019 Sesto Fiorentino, Italy.

[d] Carbon Bionanotechnology Group, CIC biomaGUNE, Parque Tecnológico de San Sebastián, Paseo Miramón, 182, 20014 San Sebastián, Guipúzcoa, Spain

*Corresponding author. Tel.: 040 5583973

E-mail address: mbevilacqua@iccom.cnr.it, pfornasiero@units.it

Abstract

The Oxygen Reduction Reaction (ORR) catalyzed by N-carbon electrocatalyst was investigated, focusing on the fundamental features for the selective H_2O_2 formation. The electrochemical characterization was primarily performed by the use of the Rotating Ring Disc Electrode (RRDE) tool in both hydrodynamic Linear Sweep Voltammetry (LSV) mode and by Chronoamperometry (CA) measurement. We rationalized the structure/activity

relationship, reaching a new state-of-the-art in terms of current density for the H_2O_2 generation. The study also explored the performance in relation with the electrode deposit procedure that is of fundamental importance to achieve a suitable macroscopic electrode preparation. Furthermore, the electrode implementation in a polymer membrane static flow electrolyzer setup, was evaluated to understand how the material catalytic features such as current ranges and selectivity scale up from a classical three electrode system to a more realistic application-focused environment.

Keywords: H_2O_2 electrosynthesis; N-carbon electrocatalyst; encapsulated Cobalt; Rotating Ring Disc Electrode

1. Introduction

The Electrochemical Hydrogen Peroxide (H_2O_2) production has undergone an increasing interest in the scientific landscape in recent years, both addressed to new electrocatalysts employment but also to enhance the multi-component structure of the electrode [1,2]. This in turn has changed how the scientific community considers H_2O_2 in the framework of the ORR, from a sub-product to a fine and high-value product [3]. Also different approaches have been proposed for a green synthesis of hydrogen peroxide, such as direct chemical routes [4] or photocatalysis [5]. However, in view of the high availability of the starting material (molecular oxygen, O_2) and the net positive current produced by the fuel cells, the ORR process has the potential to replace the energy-intensive anthraquinone process [6], still in use today, while decentralizing production. Various catalysts have been reported with high selectivity toward H_2O_2, both metal-free [7–15] or based on transition metals [16–21]. Among the studied electrolytes, alkaline conditions usually allow for higher currents trading-off on lower stability of the peroxide produced [22,23]. Neutral pH is preferred for medical

H_2O_2 applications. Finally, acidic environments combine improved peroxide stability with good throughput. Recently, this reaction has been investigated through the use of different nanocomposite materials based on N-doped carbon and earth-abundant metals, such as nickel, iron and cobalt.[24] Cobalt-carbon core shells were deemed to be the most selective for the 2-electron pathway, and it was also highlighted that the choice of the carbon precursor is of great importance: depending on the carbon precursors and on the pyrolysis temperature, graphitic carbon shells with different texture, N doping concentrations and type of the N species (pyrrolic, pyridinic, etc) are obtained. All these parameters profoundly affect both activity and selectivity, as reported in many studies [25–27]. Here we describe an in-depth analysis of the ORR framework in acidic environment when Co encapsulated N-carbon was used as electrocatalyst, focusing on the essential features for the selective H_2O_2 formation. An electrochemical investigation was performed by the use of the RRDE tool in both hydrodynamic LSV mode, as well as by CA measurement. We then rationalized the structure/activity relationship so that tailoring of the catalyst structure could lead to optimum ORR performance, reaching a new state-of-the-art in terms of current density for the H_2O_2 formation. The relationship between performance and electrode deposit protocol was also an objective of the present investigation, given its criticality for achieving suitable macroscopic electrode preparation. Finally, the material was tested in a polymer membrane static flow electrolyzer to understand how selectivities and current densities would scale in a more realistic environment.

2. Experimental

2.1. Materials

Cobalt acetate [$Co(ac)_2 \cdot 4\ H_2O$], perchloric acid ($HClO_4$), and isopropyl alcohol (99.5 %) were purchased from Carlo Erba. Melamine, sulfuric acid (H_2SO_4, 98%) and Nafion 117 solution

were purchased from Sigma–Aldrich. All reagents were used as received. All experiments were conducted with milliQ water obtained by using a Direct- Q (Millipore) water purification system.

2.2 Synthesis of Co-NCNS-T

Cobalt acetate dihydrate and melamine were first mixed in 1:1 mass ratio in a few mL of water for half an hour and then dried at 90 °C for 2 h. The powders were transferred in an open alumina vessel and kept first under Ar flow for 1.5 h at 40 °C and then 3 h at the final temperature with a fixed ramp of 3 °C/min. After cooling under Ar atmosphere, the material was dispersed in 1 M $HClO_4$ and subsequently stirred at 80 °C for 4 h. The acid-treated sample was filtered and washed with bi-distilled water. The procedure was repeated a second time and then the obtained black powder was dried under vacuum overnight and recovered. The samples were named Co-NCNSs-T, with T indicating the pyrolysis temperature. Investigated temperatures were 650, 800 and 900 °C.

2.3 Electrochemical measurements

The ORR performances were firstly evaluated at room temperature on an Autolab 302 N electrochemical workstation (Metrohm), by using a standard three-electrode setup. A GC/Pt rotating ring disk electrode (RRDE Autolab, Metrohm, geometric SA 0,196 cm^2) was used as the working electrode. A Pt plate and a saturated calomel electrode (SCE, KCl sat.), counter and reference electrodes respectively, were separated from the main chamber via bridges equipped with Vycor® frits.

To analyse H_2O_2 production, LSVs and CAs measurements on the RRDE setup were performed. The widely used Koutechy–Levich (KL) method was not deemed suitable to determine the electron transfer number as showed in literature.[28] The collection efficiency

(N_c) of the RRDE tip was evaluated for every material and rotation speed tested, showing fluctuation between the manufacturer value (25%) and 19% due to the roughness of carbon nanocomposite thin films.

All the inks were prepared in a 3:1 H_2O iPrOH mixture with the addition of 5%(v/v) Nafion® 117 solution and catalyst concentration of 2.5 mg ml^{-1}. The dispersion concentration was fixed to 2.5 mg ml^{-1}. The ink was drop casted on the polished GC-RRDE in 5 µl drops till a loading of 127.5 µg cm^{-2} was reached for every experiment, unless otherwise stated, and dried under reduced pressure.

In accordance to half- cell measurements, a further investigation of the different Co-based electrocatalysts was performed in a polymer membrane -exploiting static flow electrolyzer. The setup consisted of two separated compartments positioned in a vertically configuration and separated by a Proton-exchange Membrane (PEM, Nafion^R 117, see Fig. 1).

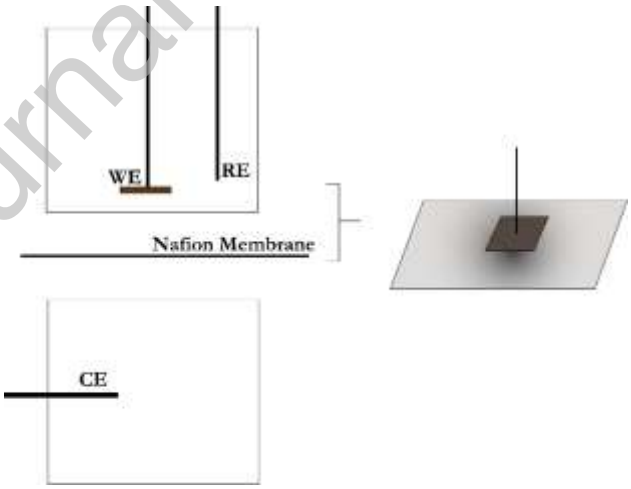

Figure 1. Schematic representation of the static flow eletrolyzer setup with side perspective of the orientation of the CP electrode with respect to the Nafion membrane.

The top compartment, i.e. the cathodic side, was characterized by a maximum volume of ~50 mL of electrolyte, saturated with O_2. The reference and the working electrode are both introduced in the top compartment of the cell, while maintaining gas-tightness, taking care that the working electrode faced downward towards the membrane and counter electrode. A Pt wire counter electrode was placed in the anodic side bottom compartment. The maximum volume of this compartment is 120 mL of electrolyte.

The catalytic material was deposited on Carbon Paper (Toray, CP) with a 2 cm^2 geometric surface area at different loadings to assess the accordance of RRDE calculated selectivity in a scaled-up system. The ink was then dried in an air furnace at 60 °C. Both sides of the CP were used for deposition. To pinch in place the CP a steel threaded rod and cap (covered from the electrolyte by a thick plastic layer) were used. The CP was pinched in the center and the area covered by the plastic cap is approximately 0.25 cm^2 on each side to be excluded from the electrode geometrical surface area.

CAs were carried out to test the catalytic stability of the Co-NCNSs in the electrolyzer setup for 1.5 h and 3 h. After bulk electrolysis, the peroxide concentration in solution was estimated through permanganometric titration (detailed information in section S1).

Both for half-cell and electrolyzer CA measurements, electrode recycling tests were performed by changing the electrolyte solution to evaluate changes in activity and/or selectivity performances with time.

2.3 Statistical Treatment

All electrochemical measurements have been replicated three times to assess reproducibility of the results. Calculated standard deviations are represented in figures as error bars and also specified in tables.

3. Results and Discussion

The Cobalt@N-doped Carbon Nano-Shell (**Co-NCNS**) were prepared by controlled pyrolysis of an appropriate cobalt derivative and melamine under argon flow. After the pyrolysis, acid washing was used to remove exohedral metal species and allowing exclusive confinement of the Co within the carbon in the final material. This aspect is critical to unequivocally assign electrocatalytic performance in core-shell systems avoiding any false conclusion arising from unaccounted presence of extra-metallic species [29]. Melamine was chosen as a carbon and nitrogen source due to its ability to form highly ordered C-N structures, such as that of graphitic carbon nitride (g-C_3N_4) [30]. In contrast with conventional g-C_3N_4 structures, the presence of the metal derivative alters the final morphology and composition, as the metal acts as a catalytic site for driving the polymerization/graphitization steps. Melamine sublimation, followed by degradation, occurs during the heating stage, favouring the formation of graphitic N-doped carbon nanospheres enveloping cobalt nanoparticles. Three different composites were prepared by varying the pyrolysis temperature (650, 800 and 900 °C) affording respectively **Co-NCNS**-650, **Co-NCNS**-800, **Co-NCNS**-900. It is known that pyrolysis temperature largely affects the properties of the material, such as morphology, composition, porosity, conductivity, and consequently the catalytic performance [31–33].

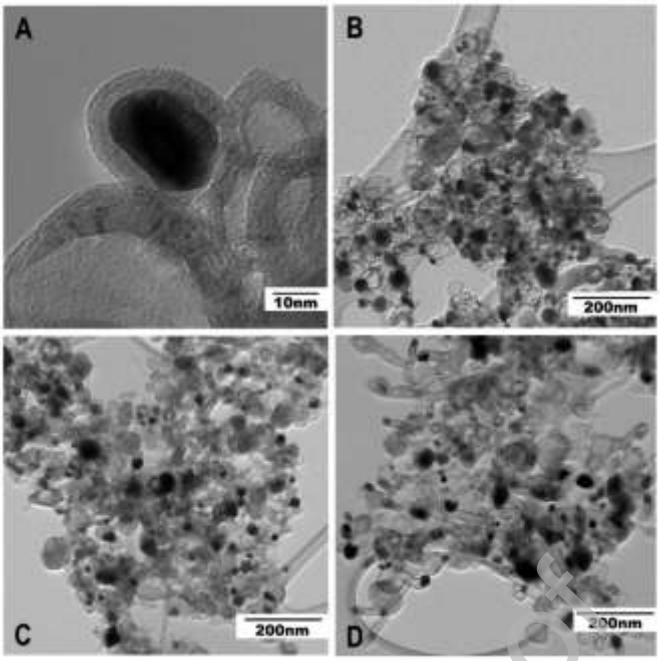

Figure 2. Typical morphology of Co-NCNS-800 visible in TEM images (a) and low magnification images of Co-NCNS-650 (b), Co-NCNS-800 (c) and Co-NCNS-900 (d).

TEM analysis (experimental details in section S2) shows that at 650 °C the preferred structure is a uniform N-doped Carbon Nano-Shell enveloping the metallic cobalt core (Fig. 2b). In contrast, higher pyrolysis temperatures (Fig. 2c and 2d) trigger to some extent the development of a carbon nanotube structure, with the Co nanoparticles located within the inner space of the nanotubes. Evidently a more severe thermal treatment allows the anisotropic catalytic growth of the carbon structure [34]. Thermogravimetric analysis (TGA, Fig. S2) shows similar characteristics throughout the Co-NCNs samples, with a stability to air until 350 °C and a residual weight of 10-15 % at 850 °C ascribed to the remaining inorganic component, while ICP-OES analysis provided a cobalt loading in the range of 4-7% (w/w).

The distribution of the nanoparticle diameters could be estimated by analysis of TEM images (Fig. S3). All three materials show broad distribution of dimensions but, with increased pyrolysis temperature, a narrowing of the distribution around a maximum of 10 nm can be seen. The high degree of graphitization of the carbon shell is supported by Raman

spectroscopy (Fig. S4), that showed a narrowing of the D and G peaks, typical of carbon material containing graphitic domains, after peak deconvolution (Figure S5), at 1320 and 1600 cm^{-1} respectively, in proportion to the higher pyrolysis temperatures, which is an indication of an increase of the graphitic character [35,36]. Moreover, the clear emergence of the double resonant peak (G') at ~ 2600 cm^{-1}, which is a signature of the graphitic sp^2 carbons [37], further supports the increasing graphitic nature with higher pyrolysis temperature. No cobalt-related peaks are visible in any sample, supporting the hypothesis that the metal is deeply clad in graphitic layers of carbon. Furthermore, the only XRD visible peaks are related to graphitic carbon and metallic cobalt (Fig. S5).

XPS analysis provided the superficial composition of the three samples (Fig. S6). Apart from N and C, a significant percentage of O is also observed, presumably introduced during the $HClO_4$ washing step (Tab. S1). Given the acid removal, observation of low-intensity peaks attributed to Co species are presumably due to some thinner carbon shell which do not prevent the core cobalt to be detected by the XPS scan depth. As expected, the increase in pyrolysis temperature results in a progressive loss of both N and O content [31,38], leading to a higher C percentage, and this is also reflected in the observed lower ORR current density with the less doped CNSs (Fig. 3, Table 1). As previously reported, the N type distribution, in particular the $N_{pyrrolic}/N_{pyridinic}$ ratio, significantly affects the ORR selectivity, with the 2-electron pathway requiring optimum $N_{pyrrolic}/N_{pyridinic}$ [33]. Accordingly, in the present case we note that pyrrolic/pyridinic ratio increases in the order Co-NCNS-650 (0.61) < Co-NCNSs-800 (0.72) < Co-NCNSs-900 (0.80), and that the best H_2O_2 selectivity is achieved with the Co-NCNSs-900 catalyst (see following discussion on electrochemistry). However, the trend in current density is the opposite, as anticipated in view of the progressive overall loss of the N and O dopants, which are typically associated with the catalytic active sites, and therefore their content is proportional with the activity [39]. Electro-Chemical Surface–area

(ECSA) and corresponding Roughness Factors (RF) confirm this tendency, showing fewer active sites for higher temperatures. It is worth to mention that even if Co is embedded within the carbon shells and therefore not directly available to the reactive environment, its indirect role in the catalysis by means of electronic surface states modification of the superficial carbon, cannot be easily dismissed, as proposed in several articles on core-shell electro-catalysts [24,29].

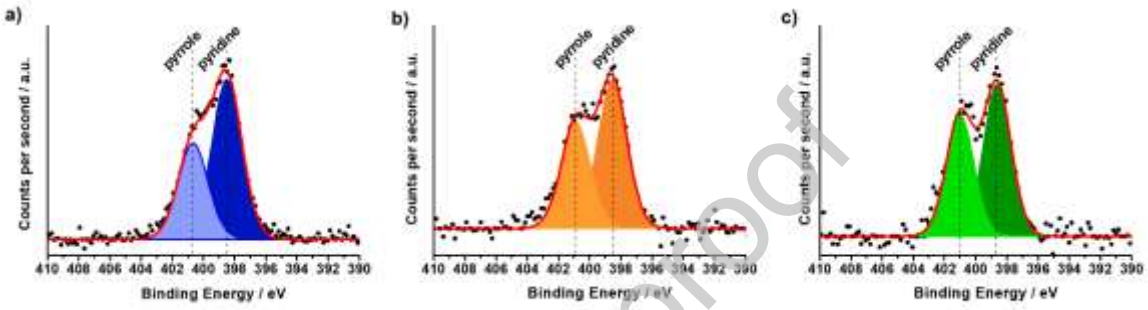

Figure 3. Deconvoluted N1s core level spectra of a) Co-NCNSs-650, b) Co-NCNSs-800, c) Co-NCNSs-900.

Samples	Pyrrolic N=C at ~401 eV (%)	Pyridinic N=C at ~398 eV (%)	Pyrrolic N=C / Pyridinic N=C
Co-NCNSs-650	37.7	62.3	0.61
Co-NCNSs-800	41.7	58.3	0.72
Co-NCNSs-900	44.4	55.6	0.80

Table 1. Atomic percentage of N1s components derived from fitting analysis.

The Brunauer–Emmett–Teller (BET) surface area decreases with higher pyrolysis temperature, as the carbon shell tends to graphitize resulting in less porous carbon (Fig. 4) [40]. Hence, the isotherms are typical of mesoporous materials, showing a hysteresis loop at high nitrogen pressures. The pore diameter distributions show two maxima, around 3 and 100 nm (Fig. S7), in which the molecular oxygen dissolved in the electrolyte can diffuse and react. Typical detrimental characteristics, such as micropores that could trap the hydrogen peroxide and favour its reduction to water [26,41], represent only a limited fraction of the pore makeup (Tab. 2).

	ECSA ***(cm^2)***	***Roughness factor***	***SA_{BET}*** ***($m^2\ g^{-1}$)***	***Ext SA*** ***($m^2\ g^{-1}$)***	***Cumulative Pore Volume*** ***($cm^3\ g^{-1}$)***	***Micropore Volume ($cm^3\ g^{-1}$)***
Co-NCNS-650	2.64±0.06	13.4±0.3	173±2	137±2	0.65	0.016
Co-NCNS-800	2.09±0.06	10.6±0.3	164±2	132±2	0.58	0.025
Co-NCNS-900	1.22±0.06	6.2±0.1	132±2	108±2	0.51	0.015

Table 2. Calculated surface areas and pore volumes derived from BET and electrochemical analysis. ECSA values are calculated on a catalytic loading of 127.5 µg cm^{-2}.

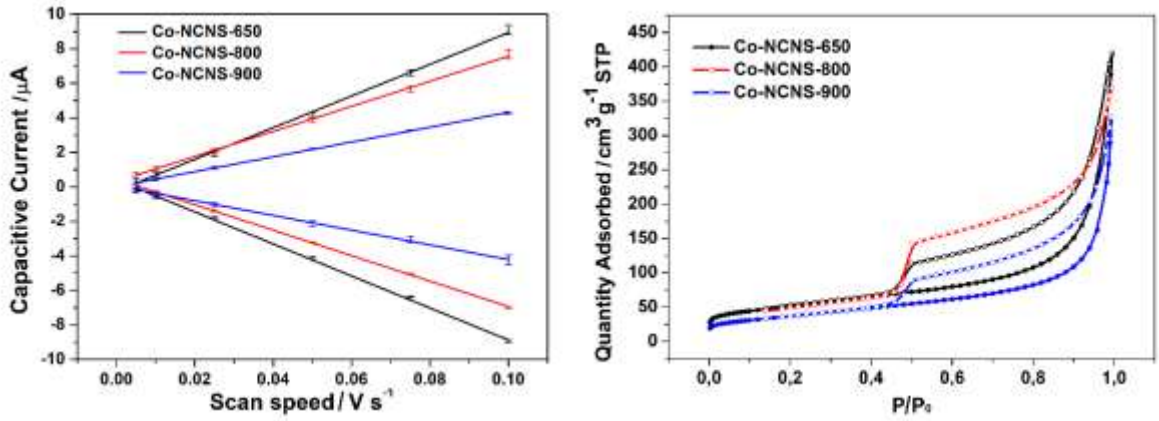

Figure 4. ECSA calculations (a), N_2 Isotherms (b) for the three synthesized Co-NCNSs

3.1 ORR performances for Co-NCNSs in half-cell

ORR catalytic activities of the different Co-C composites were investigated in relation to the pyrolysis temperature via LSV in acidic electrolyte (0.1 M H_2SO_4) between 0.9 and 0 V vs RHE at a scan rate of 5 mV s^{-1} (Fig. 5). The best catalyst loading to ensure good H_2O_2 selectivity and high current densities was determined to be 127.5 µg cm^{-2}, corresponding to a very low loading of ~6 μg_{Co} cm^{-2}, similar to state of the art catalyst loadings with precious metals in H_2O_2 generation [42].

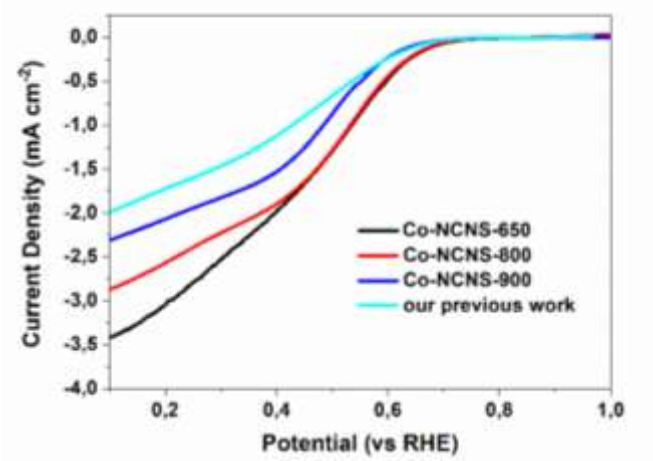

Figure 5. LSV obtained at 1600 rpm on different Co-NCNCSs compared to our previous work on cobalt core-shell systems [24].

The later onset shown by Co-NCNS-900 could be due to a lower porosity of the carbon shell (as underlined in BET and ECSA analysis) and different N-type species on the carbon surface [40]. Co-NCNSs-650, on the other hand, accounted for higher currents, presumably resulting from the higher N content, but low selectivity due to low graphitization of the material combined with the non-optimum N type distribution [33]. The above results suggested that an intermediate structure where all the chemical and structural features could be tailored for best activity and selectivity was hinged to the pyrolysis temperature. Hence, Co-NCNSs-800 was prepared to balance selectivity and throughput. The selectivity of the material was calculated from RRDE analysis and finally validated by the traditional permanganometric titration of the electrolyte.

The selectivity toward the 2-electron pathway from RRDE analysis (Fig. 6) showed that Co-NCNS-900 and Co-NCNS-800 have higher selectivity toward H_2O_2 with a peak very close to 100% at very low overpotentials; on the other hand, Co-NCNS-650 displayed higher peak currents but with substantially lower selectivity at all potentials. At high currents, all

materials tend to lose selectivity due to faster reduction kinetics (hydrogen peroxide to water) at the electrode surface [43,44].

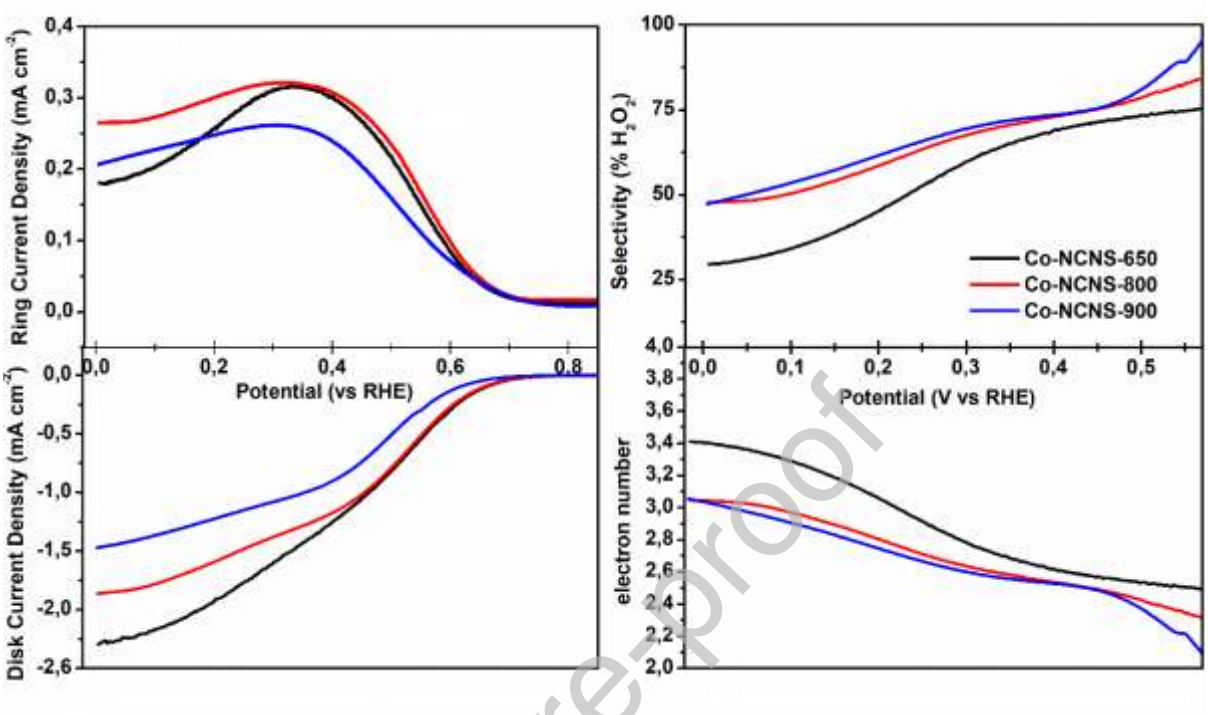

Figure 6. RRDE analysis on different Co-NCNS: Disk and Ring currents at 800 rpm (left) and calculated electron number and H_2O_2 selectivity (right).

CA tests in acidic electrolyte were employed to assess the catalytic stability of the materials. All Co-NCNS showed similar stabilities, with a retained activity higher than 95% after a 1 h test (Fig. 7). An Ion Coupled Plasma (ICP-OEP) analysis of the electrolyte after a CA test showed no traces of cobalt, excluding leaching of the cobalt core in solution. A possible deactivation route could be the reduction of catalytically active sites on the carbon surface or the loss of contact of the material on the GC interface. To further understand the surface modifications during catalysis, Co-NCNS-800 was subjected to a series of three CAs replacing the electrolyte between runs (Fig. S9). The material partial reactivation after electrolyte recycling suggests a convergence of concomitant causes: a partial deactivation of the catalyst that is reversed at the end of each CA and an irreversible reorganization or

detachment of the nanoparticles, that has been confirmed both through ECSA and RRDE collection efficiency calculations before and after a 2 h CA run (Tab. 3). The increase in collection efficiency of the RRDE (toward the 25% stated by the manufacturer) reflects a plainer surface on the electrode, resulting in diminished turbulent flow at the GCE interface. The slight loss in electrochemically active surface area is consistent with this thesis, pointing to aggregation on the surface of the electrode or detachment of the material itself.

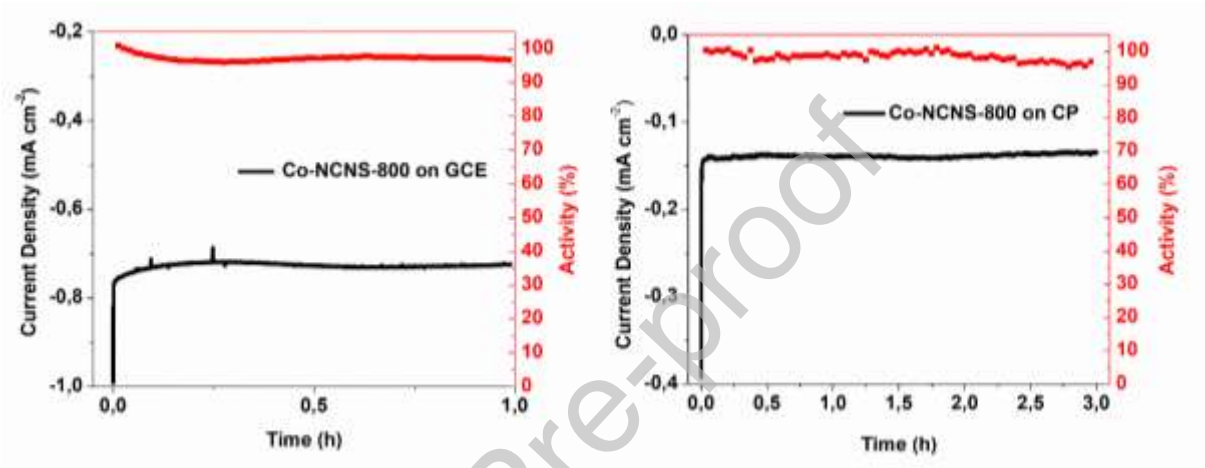

Figure 7. CA tests for Co-NCNS-800 on GC-RDE at 800 rpm (127.5 μg cm^{-2}, left) and on carbon paper (175 μg cm^{-2}, right) with calculated retained activity (as percentage).

	Before CA	***After CA***
ECSA (cm^2)	3.4±0.1	3.2±0.3
N_c (%)	19±1	24±1

Table 3. Variation of Electrochemical Surface Area (ECSA) and collection efficiency (Nc) before and after a 1 h chronoamperometry on a GC-RRDE.

3.2 Electrolyzer performance

Electrolyzer performances have been evaluated through longer CAs (3 h) and electrolyte recycling tests to understand catalytic stability in a scaled-up environment and changes in selectivity after prolonged activity. Co-NCNS-800 deposited on a CP electrode shows excellent stability both after a 3 h CA (Fig. 7) and a 6h recycling test (Fig. S9). The selectivities obtained through permanganometric titration of the electrolyte at the end of each CA test (selected data in Tab. 4; extended series of data in Table S2) showed a decrease for longer activity time, probably due to accumulation of hydrogen peroxide that can be further reduced to water at the electrode surface.

Electrode loading (μg cm^{-2})		
175	250	500
FE (H_2O_2) % [vs. Electrolysis time (h)]		
94±4 [1.5, first cycle]	82±3 [1.5, first cycle]	75±1 [1.5, first cycle]
94±4 [1.5, second cycle]	79±2 [1.5, second cycle]	74±1 [1.5, second cycle]
86±3 [3.0, third cycle]	76±3 [3.0, third cycle]	75±2 [3.0, third cycle]

Table 4. Electrode loading effect on Co-NCNS-800 selectivity toward hydrogen peroxide during electrolyte recycling tests (FE, Faradaic Efficiency).

Electrolyzer performances can be also compared to RRDE results for different loadings of Co-NCNS-800 (Fig. S8). In general, the downward trend of selectivity with higher catalytic loading is similar in both sets of experiments and in accord with literature [45]. Interestingly, from a H_2O_2 selectivity point of view, Co-NCNS-800 performs systematically better in the

electrolyzer setup (Fig. 8). The morphologic changes observed on the GCE substrate (Tab. 3) could explain better results obtained on CP. Given the flat surface of GC, CP textural properties could be of paramount importance in the stabilization of Co-NCNSs to avoid aggregation on the electrode surface.

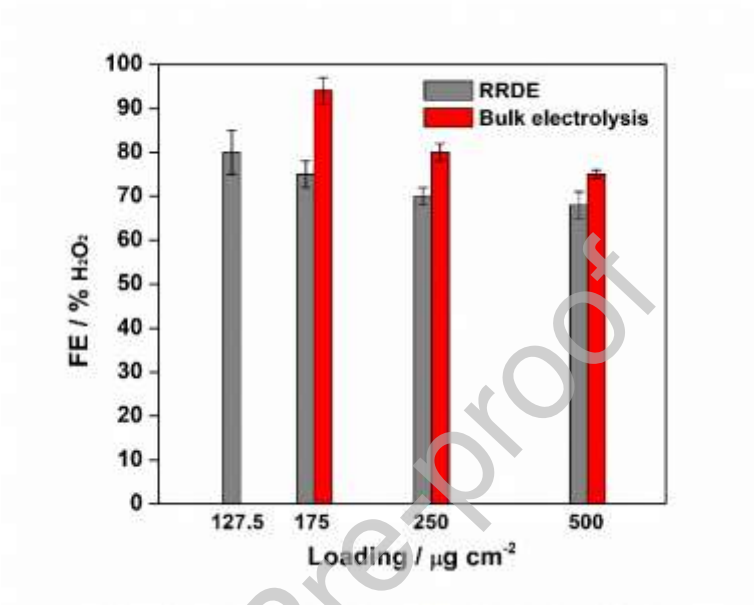

Figure 8. Data comparison between H_2O_2 FEs obtained from RRDE readings and permanganometric titrations on bulk electrolytic tests for Co-NCNS-800 at 0.5 V vs RHE with different catalytic loadings. FE referred to 127.5 μg cm^{-2} was reported only for RRDE setup cause of imperfect coverage of CP electrode with the same ink formulation.

4. Conclusions

ORR catalytic activities of three different Co-C composites (Co-NCNS-T) were firstly investigated in a half-cell setup in relation to the pyrolysis temperature via LSV in acidic electrolyte (0.1 M H_2SO_4). RRDE measurements showed the superior selectivity towards H_2O_2 by Co-NCNS-900 and Co-NCNS-800, almost close to completeness under optimized conditions, even though peak currents are lower as compared to Co-NCNS-650. Co-NCNS-

800 was subjected to a deeper investigation by performing multiple CAs replacing the electrolyte between runs and parallel ECSA measurements; such a combination of experiments allowed to attribute the loss of electrochemical performance to a physical surface electrode modification Co-NCNS-800 was further investigated by means of a superior setup based on an electrolyzer configuration, showing excellent stability both after a 3 h CA and a 6 h recycling test. The calculated bulk electrolysis (CA experiments) selectivity exhibited a slight decrease for longer operation times, probably due to accumulation of H_2O_2 that can be further reduced to water at the electrode surface. The results obtained herein pave the way to a rational design of flow – electrolyzer and MEA-based devices towards a real scale up for faster transfer to industrial utilization stage. Optimized working conditions related to the multi-layer structure of a PEM/MEA-structured electrolyzer and multilayer electrolyzer stacks represent one of the main targets to address H_2O_2 supply on industrial scale production by means of electrochemical methods.

Acknowledgements: This work was supported by the MAECI - MOST – Italy- China CN19GR04 and Italian MIUR through the PRIN 2017 (2017YH9MRK) "Novel Multilayered and Micro-Machined Electrode Nano-Architectures for Electrocatalytic Applications (Fuel Cells and Electrolyzers)". University of Trieste, INSTM and ICCOM-CNR are acknowledged for financial support.

References

[1] A.T. Murray, S. Voskian, M. Schreier, T.A. Hatton, Y. Surendranath, Electrosynthesis of Hydrogen Peroxide by Phase-Transfer Catalysis, Joule. 3 (2019) 2942–2954.

[2] Q. Zhang, M. Zhou, G. Ren, Y. Li, Y. Li, X. Du, Highly efficient electrosynthesis of

hydrogen peroxide on a superhydrophobic three-phase interface by natural air diffusion, Nat. Commun. 11 (2020) 1–11.

[3] A. Verdaguer-Casadevall, D. Deiana, M. Karamad, S. Siahrostami, P. Malacrida, T.W. Hansen, J. Rossmeisl, I. Chorkendorff, I.E.L. Stephens, Trends in the electrochemical synthesis of H_2O_2: Enhancing activity and selectivity by electrocatalytic site engineering, Nano Lett. 14 (2014) 1603–1608.

[4] J.M. Campos-Martin, G. Blanco-Brieva, J.L.G. Fierro, Hydrogen peroxide synthesis: An outlook beyond the anthraquinone process, Angew. Chemie - Int. Ed. 45 (2006) 6962–6984.

[5] H. Hou, X. Zeng, X. Zhang, Production of Hydrogen Peroxide by Photocatalytic Processes, Angew. Chemie Int. Ed. 59 (2020) 17356–17376.

[6] H.J.R. G. Pfleiderer, US2158525A, 1939.

[7] T.P. Fellinger, F. Hasché, P. Strasser, M. Antonietti, Mesoporous nitrogen-doped carbon for the electrocatalytic synthesis of hydrogen peroxide, J. Am. Chem. Soc. 134 (2012) 4072–4075.

[8] Y. Liu, X. Quan, X. Fan, H. Wang, S. Chen, High-Yield Electrosynthesis of Hydrogen Peroxide from Oxygen Reduction by Hierarchically Porous Carbon, Angew. Chemie Int. Ed. 54 (2015) 6837–6841.

[9] Z. Lu, G. Chen, S. Siahrostami, Z. Chen, K. Liu, J. Xie, L. Liao, T. Wu, D. Lin, Y. Liu, T.F. Jaramillo, J.K. Nørskov, Y. Cui, High-efficiency oxygen reduction to hydrogen peroxide catalysed by oxidized carbon materials, Nat. Catal. 1 (2018) 156–162.

[10] Y. Sun, I. Sinev, W. Ju, A. Bergmann, S. Dresp, S. Kühl, C. Spöri, H. Schmies, H.

Wang, D. Bernsmeier, B. Paul, R. Schmack, R. Kraehnert, B. Roldan Cuenya, P. Strasser, Efficient Electrochemical Hydrogen Peroxide Production from Molecular Oxygen on Nitrogen-Doped Mesoporous Carbon Catalysts, ACS Catal. 8 (2018) 2844–2856.

[11] S. Chen, Z. Chen, S. Siahrostami, D. Higgins, D. Nordlund, D. Sokaras, T.R. Kim, Y. Liu, X. Yan, E. Nilsson, R. Sinclair, J.K. Nørskov, T.F. Jaramillo, Z. Bao, Designing Boron Nitride Islands in Carbon Materials for Efficient Electrochemical Synthesis of Hydrogen Peroxide, J. Am. Chem. Soc. 140 (2018) 7851–7859.

[12] L. Han, Y. Sun, S. Li, C. Cheng, C.E. Halbig, P. Feicht, J.L. Hübner, P. Strasser, S. Eigler, In-Plane Carbon Lattice-Defect Regulating Electrochemical Oxygen Reduction to Hydrogen Peroxide Production over Nitrogen-Doped Graphene, ACS Catal. 9 (2019) 1283–1288.

[13] W. Wang, X. Lu, P. Su, Y. Li, J. Cai, Q. Zhang, M. Zhou, O. Arotiba, Enhancement of hydrogen peroxide production by electrochemical reduction of oxygen on carbon nanotubes modified with fluorine, Chemosphere. 259 (2020) 127423.

[14] L.Z. Peng, P. Liu, Q.Q. Cheng, W.J. Hu, Y.A. Liu, J.S. Li, B. Jiang, X.S. Jia, H. Yang, K. Wen, Highly effective electrosynthesis of hydrogen peroxide from oxygen on a redox-active cationic covalent triazine network, Chem. Commun. 54 (2018) 4433–4436.

[15] K.H. Wu, D. Wang, X. Lu, X. Zhang, Z. Xie, Y. Liu, B.J. Su, J.M. Chen, D.S. Su, W. Qi, S. Guo, Highly Selective Hydrogen Peroxide Electrosynthesis on Carbon: In Situ Interface Engineering with Surfactants, Chem. 6 (2020) 1443–1458.

[16] S. Siahrostami, A. Verdaguer-Casadevall, M. Karamad, D. Deiana, P. Malacrida, B. Wickman, M. Escudero-Escribano, E.A. Paoli, R. Frydendal, T.W. Hansen, I.

Chorkendorff, I.E.L. Stephens, J. Rossmeisl, Enabling direct H2O2 production through rational electrocatalyst design, Nat. Mater. 12 (2013) 1137–1143.

[17] W.W. Zhao, P. Bothra, Z. Lu, Y. Li, L.P. Mei, K. Liu, Z. Zhao, G. Chen, S. Back, S. Siahrostami, A. Kulkarni, J.K. Nørskov, M. Bajdich, Y. Cui, Improved Oxygen Reduction Reaction Activity of Nanostructured CoS_2 through Electrochemical Tuning, ACS Appl. Energy Mater. 2 (2019) 8605–8614.

[18] J. Gao, H. bin Yang, X. Huang, S.F. Hung, W. Cai, C. Jia, S. Miao, H.M. Chen, X. Yang, Y. Huang, T. Zhang, B. Liu, Enabling Direct H_2O_2 Production in Acidic Media through Rational Design of Transition Metal Single Atom Catalyst, Chem. 6 (2020) 658–674.

[19] C. Tang, Y. Jiao, B. Shi, J. Liu, Z. Xie, X. Chen, Q. Zhang, S. Qiao, Coordination Tunes Selectivity: Two- Electron Oxygen Reduction on High- Loading Molybdenum Single- Atom Catalysts, Angew. Chemie Int. Ed. 59 (2020) 9171–9176.

[20] S. Kralj, F. Longobardo, D. Iglesias, M. Bevilacqua, C. Tavagnacco, A. Criado, J.J. Delgado Jaen, D. Makovec, S. Marchesan, M. Melchionna, M. Prato, P. Fornasiero, Ex-Solution Synthesis of Sub-5-nm FeO_x Nanoparticles on Mesoporous Hollow N,O-Doped Carbon Nanoshells for Electrocatalytic Oxygen Reduction, ACS Appl. Nano Mater. 2 (2019) 6092–6097.

[21] V.S. Antonin, L.S. Parreira, L.R. Aveiro, F.L. Silva, R.B. Valim, P. Hammer, M.R.V. Lanza, M.C. Santos, W@Au Nanostructures Modifying Carbon as Materials for Hydrogen Peroxide Electrogeneration, Electrochim. Acta. 231 (2017) 713–720.

[22] Z. Chen, S. Chen, S. Siahrostami, P. Chakthranont, C. Hahn, D. Nordlund, S. Dimosthenis, J.K. Nørskov, Z. Bao, T.F. Jaramillo, Development of a reactor with carbon catalysts for modular-scale, low-cost electrochemical generation of H_2O_2,

React. Chem. Eng. 2 (2017) 239–245.

[23] W.D. Nicoll, A.F. Smith, Stability of Dilute Alkaline Solutions of Hydrogen Peroxide, Ind. Eng. Chem. 47 (1955) 2548–2554.

[24] A. Lenarda, M. Bevilacqua, C. Tavagnacco, L. Nasi, A. Criado, F. Vizza, M. Melchionna, M. Prato, P. Fornasiero, Selective Electrocatalytic H_2O_2 Generation by Cobalt@N-Doped Graphitic Carbon Core–Shell Nanohybrids, ChemSusChem. 12 (2019) 1664–1672.

[25] S. Kundu, T.C. Nagaiah, W. Xia, Y. Wang, S. Van Dommele, J.H. Bitter, M. Santa, G. Grundmeier, M. Bron, W. Schuhmann, M. Muhler, Electrocatalytic activity and stability of nitrogen-containing carbon nanotubes in the oxygen reduction reaction, J. Phys. Chem. C. 113 (2009) 14302–14310.

[26] W. He, C. Jiang, J. Wang, L. Lu, High-rate oxygen electroreduction over graphitic-N species exposed on 3D hierarchically porous nitrogen-doped carbons, Angew. Chemie - Int. Ed. 53 (2014) 9503–9507.

[27] G. Tuci, C. Zafferoni, P. D'Ambrosio, S. Caporali, M. Ceppatelli, A. Rossin, T. Tsoufis, M. Innocenti, G. Giambastiani, Tailoring carbon nanotube N-dopants while designing metal-free electrocatalysts for the oxygen reduction reaction in alkaline medium, ACS Catal. 3 (2013) 2108–2111.

[28] R. Zhou, Y. Zheng, M. Jaroniec, S.-Z. Qiao, Determination of the Electron Transfer Number for the Oxygen Reduction Reaction: From Theory to Experiment, ACS Catal. 6 (2016) 4720–4728.

[29] M. Melchionna, P. Fornasiero, M. Prato, Into the carbon: A matter of core and shell in advanced electrocatalysis, APL Mater. 8 (2020) 020905.

[30] A. Thomas, A. Fischer, F. Goettmann, M. Antonietti, J.O. Müller, R. Schlögl, J.M. Carlsson, Graphitic carbon nitride materials: Variation of structure and morphology and their use as metal-free catalysts, J. Mater. Chem. 18 (2008) 4893–4908.

[31] A.A. Koós, A.T. Murdock, P. Nemes-Incze, R.J. Nicholls, A.J. Pollard, S.J. Spencer, A.G. Shard, D. Roy, L.P. Biró, N. Grobert, Effects of temperature and ammonia flow rate on the chemical vapour deposition growth of nitrogen-doped graphene, Phys. Chem. Chem. Phys. 16 (2014) 19446–19452.

[32] H. Yu, L. Shang, T. Bian, R. Shi, G.I.N. Waterhouse, Y. Zhao, C. Zhou, L.Z. Wu, C.H. Tung, T. Zhang, Nitrogen-Doped Porous Carbon Nanosheets Templated from g-C3N4as Metal-Free Electrocatalysts for Efficient Oxygen Reduction Reaction, Adv. Mater. 28 (2016) 5080–5086.

[33] D. Iglesias, A. Giuliani, M. Melchionna, S. Marchesan, A. Criado, L. Nasi, M. Bevilacqua, C. Tavagnacco, F. Vizza, M. Prato, P. Fornasiero, N-Doped Graphitized Carbon Nanohorns as a Forefront Electrocatalyst in Highly Selective O_2 Reduction to H_2O_2, Chem. 4 (2018) 106–123.

[34] D. Iglesias, M. Melchionna, Enter the Tubes: Carbon Nanotube Endohedral Catalysis, Catalysts. 9 (2019) 128.

[35] A. Ferrari, J. Robertson, Interpretation of Raman spectra of disordered and amorphous carbon, Phys. Rev. B - Condens. Matter Mater. Phys. 61 (2000) 14095–14107.

[36] A.C. Ferrari, J. Robertson, Raman spectroscopy of amorphous, nanostructured, diamond–like carbon, and nanodiamond, Philos. Trans. R. Soc. London. Ser. A Math. Phys. Eng. Sci. 362 (2004) 2477–2512.

[37] M.S. Dresselhaus, A. Jorio, M. Hofmann, G. Dresselhaus, R. Saito, Perspectives on

carbon nanotubes and graphene Raman spectroscopy, Nano Lett. 10 (2010) 751–758.

[38] A. Dorjgotov, J. Ok, Y.K. Jeon, S.H. Yoon, Y.G. Shul, Activity and active sites of nitrogen-doped carbon nanotubes for oxygen reduction reaction, J. Appl. Electrochem. 43 (2013) 387–397.

[39] M. Melchionna, P. Fornasiero, M. Prato, The Rise of Hydrogen Peroxide as the Main Product by Metal- Free Catalysis in Oxygen Reductions, Adv. Mater. 31 (2019) 1802920.

[40] Z. Zhou, T. Liu, A.U. Khan, G. Liu, Controlling the physical and electrochemical properties of block copolymer-based porous carbon fibers by pyrolysis temperature, Mol. Syst. Des. Eng. 5 (2020) 153–165.

[41] J. Liang, X. Du, C. Gibson, X.W. Du, S.Z. Qiao, N-doped graphene natively grown on hierarchical ordered porous carbon for enhanced oxygen reduction, Adv. Mater. 25 (2013) 6226–6231.

[42] R. Shen, W. Chen, Q. Peng, S. Lu, L. Zheng, X. Cao, Y. Wang, W. Zhu, J. Zhang, Z. Zhuang, C. Chen, D. Wang, Y. Li, High-Concentration Single Atomic Pt Sites on Hollow CuS_x for Selective O_2 Reduction to H_2O_2 in Acid Solution, Chem. 5 (2019) 2099–2110.

[43] A. Kozawa, V.E. Zilionis, R.J. Brodd, Oxygen and Hydrogen Peroxide Reduction at a Ferric Phthalocyanine-Catalyzed Graphite Electrode, J. Electrochem. Soc. 117 (1970) 1470.

[44] A.J. Appleby, Electrocatalysis of aqueous dioxygen reduction, J. Electroanal. Chem. 357 (1993) 117–179.

[45] E.J. Biddinger, D. von Deak, D. Singh, H. Marsh, B. Tan, D.S. Knapke, U.S. Ozkan,

Examination of Catalyst Loading Effects on the Selectivity of CNx and Pt/VC ORR Catalysts Using RRDE, J. Electrochem. Soc. 158 (2011) B402.

Authors Credit

Marcello Ferrara performed, elaborated and discussed electrochemical data, contribute to write the draft.

Manuela Bevilacqua designed the electrochemical experiments, performed, elaborated and discussed electrochemical data, contribute to write the draft.

Michele Melchionna performed, elaborated and discussed Raman and N_2 physisorption data, contribute to write the draft.

Alejandro Criado performed, elaborated and discussed XPS data

Matteo Crosera performed, elaborated and discussed ICP-OES data

Claudio Tavagnacco discussed and supervised the electrochemical experiments

Francesco Vizza supported the research and contributed to coordinate the activities

Paolo Fornasiero coordinate the activities, supervised the research and supported the research

All authors read and discussed the manuscript

Declaration of interests

The authors declare that they have no known competing financial interests or personal relationships that could have appeared to influence the work reported in this paper.